NbZr multilayers. II. Extended x-ray-absorption fine-structure study

T. Claeson
Physics Department, Chalmers University of Technology, S-412 96 Gothenburg, Sweden

J. B. Boyce
Xerox Palo Alto Research Center, Palo Alto, California 94304

W. P. Lowe and T. H. Geballe
Department of Applied Physics, Stanford University, Stanford, California 94305
(Received 18 April 1983; revised manuscript received 1 August 1983)

Extended x-ray-absorption fine-structure (EXAFS) measurements have been used to study the atomic-scale structure of a series of ten multilayer films of NbZr with layer-spacing periods Λ ranging from 4 to 200 Å. It is found that the Zr layers have a gradual hcp-to-bcc transformation as the layer-spacing period decreases, being predominately hcp for $\Lambda \gg 50$ Å and predominately bcc for $\Lambda \ll 50$ Å. It is also shown that the layers are not sharp but rather that there is significant interdiffusion. Assuming that one multilayer period contains two interdiffusive layers at the boundaries between the two constituent films, we estimate that diffusion lengths of Nb into Zr and Zr into Nb at the interlayer are about 15 Å for sputtered NbZr multilayers.

I. INTRODUCTION

Although studied less than their semiconducting relatives, multilayers of metal films exhibit some interesting phenomena in, e.g., their mechanical[1] and magnetic[2] properties. Soft phonons and additional interactions[3] at the interfaces may, furthermore, enhance superconductivity. Structurewise, it has been proposed that the atomic positions in the different films are positioned in such a way as to give a coherent structure in the multilayer, with the structure of one of the constituent films being pulled to the same symmetry as the other if the films are thin enough.[4]

Extended x-ray-absorption fine structure (EXAFS) is an excellent method to study the local environment of atoms.[5] The average number of different neighbors, their distances to the absorbing atom, and the spread in distances, can be estimated. This study has combined x-ray, EXAFS, and superconductivity information to characterize multilayers of Nb and Zr films fabricated by a sputtering process. Here, we concentrate on the EXAFS results to show that the technique is applicable in the study of interfaces, and that the hcp Zr is indeed transformed into a bcc phase for small multilayer periods. These EXAFS results are compared, where appropriate, to the x-ray diffraction results contained in Ref. 6.

II. SAMPLE PREPARATION AND CHARACTERIZATION

Samples were made by sputtering from two well-separated Nb and Zr electrodes.[7] Substrates of kapton (for the EXAFS experiment) and sapphire (for the x-ray-scattering and superconductivity experiments) were clamped to a table rotating below the electrodes. The sputtering rates were adjusted to give equal thicknesses of the two constituents as the table passed by. The amount of deposited material depended on how rapidly the substrates passed the electrodes and also on the sputtering rate from each source. By varying the speed of the table rotation, periods Λ of 4—200 Å were realized. Standard samples of dilute solutions of Nb in Zr and Zr in Nb were made in a separate sputtering unit operated in the phase-spread mode. All films were deposited at room temperature. Some of the materials prepared on kapton were checked using x-ray diffraction to verify that the sample characteristics were substrate independent.

Microprobe measurements showed (in agreement with the absorption-edge steps in our experiment) that the Nb:Zr ratio was indeed about 1:1, with the largest deviation being 45:55 for the $\Lambda = 31$ Å sample. The x-ray-diffraction results[6] indicate that the films were strongly textured with the [002] direction perpendicular to the film plane for hcp Zr and the [110] direction perpendicular to the film plane for the bcc Nb film. The x-ray lines at small angle exhibited satellites, the separation of which confirmed the layer spacing expected from the fabrication process. From the widths of the satellite lines we conclude that the layer thicknesses are uniform throughout the samples. For small Λ, only the first pair of satellites were clearly seen. This indicates that the concentrations of Nb and Zr do not change abruptly at the interfaces, but rather they change more smoothly. Satellites were seen also in the small-Λ samples, at least down to $\Lambda = 13$ Å, indicating a modulation even on a fine scale.

Both the hcp and bcc x-ray-diffraction lines were seen. From these we could determine lattice constants as needed for this study. The hcp-line intensity decreased rapidly for Λ less than 50 Å, indicating that the structure for $\Lambda < 50$ Å is predominately bcc. No hcp line was seen for $\Lambda = 19$ Å, but a weak line that could be indexed as hcp appeared for the $\Lambda = 4$ Å sample.

The uniform periodicity was verified by secondary-ion mass spectroscopy (SIMS). The high energy of the impinging sputtering ions in that method, however, limits the depth resolution, and no detailed information of the concentration profile at the interface could be obtained. For the $\Lambda=200$ Å sample, SIMS shows that the outermost Zr film contained no Nb, at least in the first 30 Å of the layer. The layering appeared clearly in the shallow etch pit left by the SIMS sputtering. It could be studied by both optical and electron microscopy.

III. EXAFS INVESTIGATION

A study of the EXAFS is well suited for the investigation of the local environments of atoms.[5,8,9] The backscattering of electrons photoexcited from the K shell of the absorbing atom A gives rise to structure in the absorption cross section, $\sigma_A(\omega)=\sigma_A^0(\omega)[1+\chi_A(\omega)]$. Assuming no multiple scattering and a polycrystalline sample, the EXAFS is given by[8]

$$\chi_A(k)=\frac{1}{k}\sum_j \frac{N_j F_j(k)}{r_j^2}\sin[2kr_j+\delta_j(k)]e^{-2r_j/\lambda-2\sigma_j^2k^2}, \tag{1}$$

where k is the wave vector of the ejected electron, $\hbar^2k^2/2m=\hbar\omega-E_{\rm th}$, $\hbar\omega$ is the photon energy, and the threshold energy $E_{\rm th}$ is given by the K edge. $F_j(k)$ is the backscattering amplitude depending upon the kind of atoms present in shell j, and $\delta_j(k)$ is a phase shift depending both on the scattering and absorbing atoms. The mean free path of the excited electron is λ. Hence $\chi_A(k)$ gives information about the number of neighbors N_j at distance r_j from the absorbing atom and the mean-square fluctuation σ_j^2 of r_j arising from structural and thermal disorder.

For this study we have analyzed the Fourier transform $\phi(r)$ of the EXAFS $k\chi(k)$, given by

$$\phi_A(r)=\sum_\beta \int_0^\infty dr'(r')^{-2}P_{A\beta}(r')\zeta_{A\beta}(r-r'), \tag{2}$$

where $P_{A\beta}$ is the pair correlation function of the absorbing atom A with the backscattering atoms β, and $\zeta_{A\beta}$ is a peak function. $P_{A\beta}$ contains the structural information of interest.[9]

A. EXAFS experimental technique

Several strips were cut from the multilayer samples sputtered on the kapton substrates. They were stacked on each other to obtain the optimal thickness of about 30 μm, i.e., about 2.5 absorption lengths. During the investigations they were cooled to 77 K in an exchange-gas atmosphere of He. The plane of the films was perpendicular to the photon-beam direction for all the films studied.

Transmission EXAFS was taken at both the Nb (19-kev) and Zr (18-keV) K edges using the facilities at the Stanford Synchrotron Radiation Laboratory (SSRL) (VII-3 Wiggler line). The radiation wavelength was varied by a Si(220) crystal monochromator and the photon energy was swept from 1000 eV below to 1600 eV above the edges. The crystal was detuned to one-half of the maximum transmitted intensity in order to reduce the fraction of higher harmonics in the beam. The incident- and the transmitted-radiation intensities were determined by ionization chambers filled with Ne gas at atmospheric pressure. Photographs of the transmitted x-rays were taken to assure there were no gross inhomogeneities in the samples.

B. EXAFS analysis

The EXAFS information was extracted from the absorptance using a standard procedure.[5,9] The slowly varying background was subtracted using a polynomial, the parameters of which were determined from the transmission at 900 to 100 eV below the edges. $\sigma^0_{\rm Nb,Zr}(\omega)$ was then approximated by a sixth-order polynomial in $(\hbar\omega-E_{\rm th})^{1/2}$ fitted from an energy just above the edge to the maximum energy. $E_{\rm th}$ was chosen as the energy at which the absorptance discontinuity at the edge had reached its half value (excluding the threshold spike). The fine-structure function was converted to k space, multiplied by k to give $k\chi(k)$, then Fourier-transformed to r space. The latter was performed over a window of 2.45–14.4 Å^{-1} for Zr absorbers and 2.7–19.3 Å for Nb. Both square windows were broadened by convolution with a Gaussian of width 0.7 Å^{-1}.

The Fourier transform $\phi(r)$ of the EXAFS, $k\chi(k)$, gives a qualitative picture of the radial distribution of neighbors. Changes in symmetry, e.g., can easily be seen. In a more quantitative analysis we can compare the real and imaginary parts of $\phi(r)$ with those calculated from theoretical backscattering potentials or with those from standards with a known structure. We have chosen the latter procedure and used sputtered Nb and Zr films or Nb and Zr foils to give Nb-Nb and Zr-Zr backscattering signatures. Nb-Zr and Zr-Nb signatures at the first-neighbor peak were obtained from sputtered dilute-alloy films where Nb (or Zr) absorbers sit in mainly a Zr (or Nb) environment. The alloy standards had bcc structures. One- or two-Gaussian fits of signatures to $\phi(r)$ of the layered samples gave the relative amplitudes (information containing the coordination numbers), the shifts in neighbor separations, and the additional Debye-Waller broadenings of the pair radial distribution functions in question, as compared to the first neighbors of the signatures.

C. EXAFS data

EXAFS oscillations of good quality were obtained for samples with modulation periods from 4 to 200 Å. Examples of $k\chi(k)$ are given in Fig. 1 for the Zr K edge. The $\Lambda=13$ Å sample had a considerably lower EXAFS amplitude (both at the Nb and Zr edges) than the others. This means that a quantitative analysis of that sample gives less reliable results than for the other multilayers. Similar difficulties were observed with this sample in the x-ray-diffraction analysis.[6] This indicates that this sample is more disordered than the others. The origin of this is not known.

Fourier transforms of the EXAFS at the Zr K edge are given in Fig. 2, while those at the Nb edge are presented in Fig. 3. Already from the data in Fig. 3 we can conclude that the crystal symmetry relative to the absorbing Nb

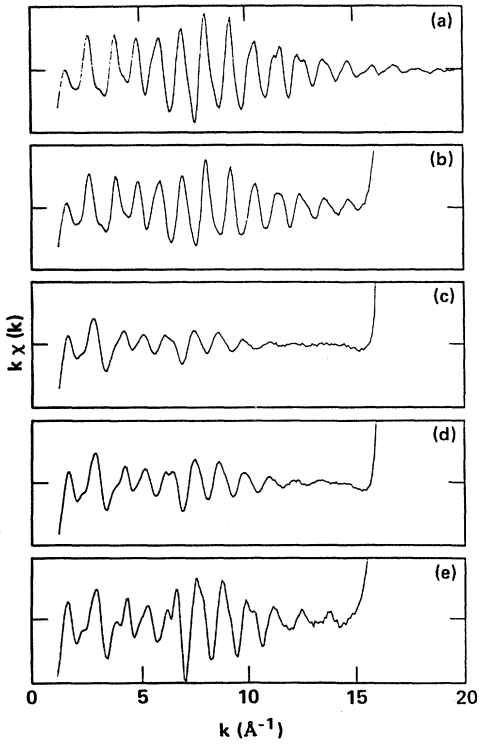

FIG. 1. EXAFS, $k\chi(k)$, on the Zr K edge for (a) the Zr film; for NbZr multilayers with (b) $\Lambda = 139$ Å, (c) $\Lambda = 19$ Å, and (d) $\Lambda = 4$ Å; and (e) the $Zr_{0.1}Nb_{0.9}$ alloy. The vertical scales in each case are the same, varying from -0.3 to $+0.3$ Å^{-1}. Note the similarity of the EXAFS for the Zr film and the multilayer film with the large layer spacing $\Lambda = 139$ Å [i.e., (a) and (b)]. The increase above 15 Å^{-1} is due to the Nb edge.

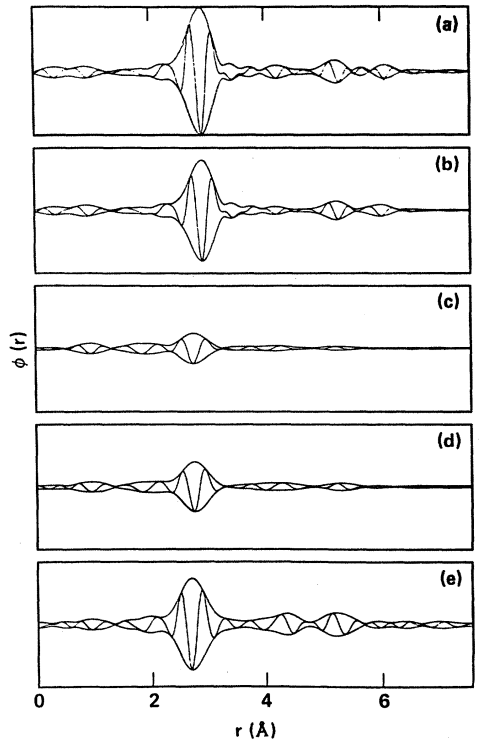

FIG. 2. Fourier transforms $\phi(r)$ of the EXAFS on the Zr K edge for the data of Fig. 1. The vertical scales in each case are the same, varying from -0.55 to $+0.55$ Å^{-2}. The transforms were performed using a square k-space window from 2.45 to 14.4 Å^{-1}, broadened by a Gaussian of width 0.7 Å^{-1}.

atoms seems to remain unchanged (bcc) as Λ is varied. The lowest r peak, which is split into a double peak by the superposition of backscattering from the first two near-neighbor shells with eight and six neighbors, respectively, is broadened into a wide peak for small Λ. Similar wide peaks appear for the Nb EXAFS of the NbZr reference alloys.

The Zr-edge EXAFS (Fig. 2), on the other hand, changes in character as the modulation length is decreased. For large Λ's, $\phi_{Zr}(r)$ is very similar to the EXAFS transforms for the pure Zr film or the foil, consistent with the lattice-constant results for these films. Peaks appear at distances corresponding to neighbors of successively higher order in the hcp structure. For the smallest values of Λ, below about 50 Å, the transforms resemble those of the bcc-alloy standards. In other words, an hcp-to-bcc transition occurs for the Zr layers below about $\Lambda = 50$ Å.

We also note that the amplitudes of $\phi(r)$ for the pure films and the layers are smaller than those for the foils. This is true both for the Nb- and Zr-edge EXAFS. Computer fits gave ratios of textured film to polycrystalline-foil amplitudes of 0.83 for Nb and 0.77 for Zr. The decrease is consistent with the texturing of the sputtered films. The synchrotron radiation is strongly polarized in a direction perpendicular to the photon-propagation vector. The EXAFS and thus the amplitude is proportional to $\sum N_i \cos^2\theta_i$, where θ_i is the angle between the photon-polarization vector and the direction to neighbor i relative to the absorber. We can obtain either an increase or a decrease of the EXAFS amplitude of a textured film compared to the polycrystalline material. It depends on which plane is parallel to the film surface. In our case, we know the orientation of both the bcc and the hcp layers. However, within a film layer there is a mosaic structure of regions that are misoriented relative to each other. If this mosaic structure is random, it will provide an effective average over all possible angles in the plane. In the bcc Nb film with the [110] direction perpendicular to the film, such an average gives the same result as a powder; that is, the amplitude ratio of the film to foil is 1, not 0.83 as observed. If, however, the misalignment between two regions is not random, it is difficult to compute the EXAFS amplitude. The measured ratio is, nonetheless, not unreasonable. In the fits, furthermore, we use the data on the textured films, not the polycrystalline foils, for both the standards and the unknowns. In this case, if the texturing of the various films is the same, then the amplitudes will be correctly determined. X-ray diffraction indicates that this is the case,[6] so no adjustments of the amplitudes need to be made.

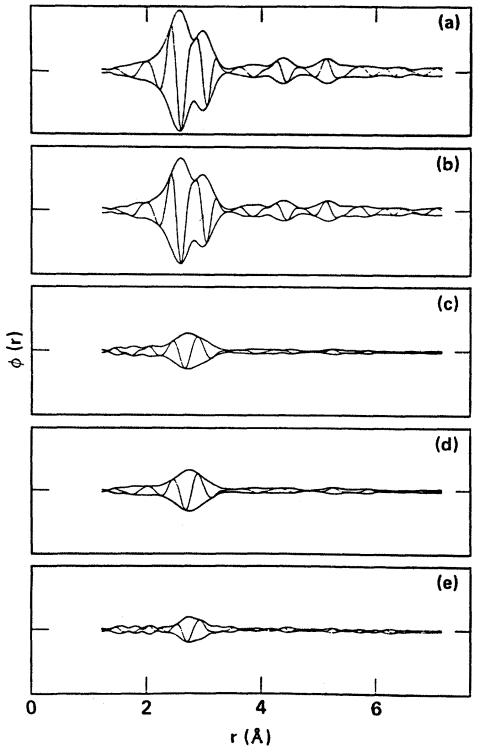

FIG. 3. Fourier transforms $\phi(r)$ of the EXAFS on the Nb K edge for (a) the Nb film; for NbZr multilayers with (b) $\Lambda=139$ Å, (c) $\Lambda=19$ Å, and (d) $\Lambda=4$ Å; and for (e) the $Nb_{0.2}Zr_{0.8}$ alloy. The vertical scales in each case are the same, varying from -0.5 to $+0.5$ Å^{-2}. The transforms were performed using a square k-space window from 2.7 to 19.3 Å^{-1}, broadened by a Gaussian of width 0.7 Å^{-1}. Note the double-peak structure in the vicinity of 2–3.5 Å for all these films, but most prominent for the Nb film and the multilayer film with $\Lambda=139$ Å [i.e., (a) and (b)]. This is due to the bcc structure of these films.

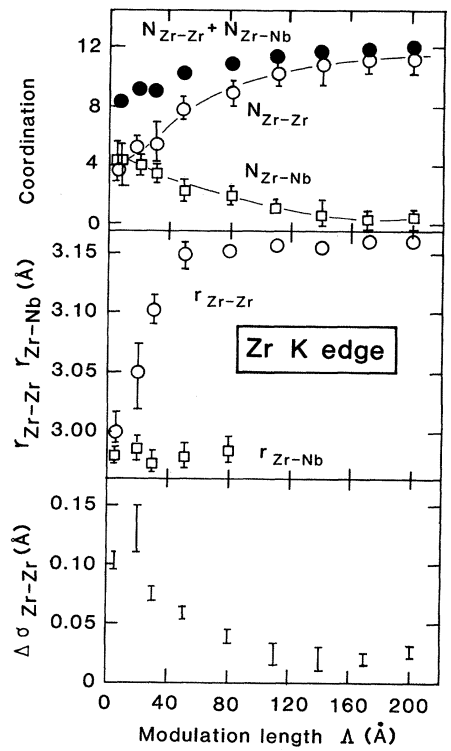

FIG. 4. Average numbers of Nb and Zr neighbors to an absorbing Zr atom as a function of modulation period are displayed in the upper part. The total average coordination number of a Zr atom is also shown. It equals 12, characteristic of an hcp structure, at large Λ, while it approaches the bcc value of 8 at small Λ due to the hcp-to-bcc transition. The middle part of the diagram gives the variations of the Zr-Zr and Zr-Nb distances. The latter becomes very uncertain when the average number of Zr-Nb pairs becomes small at large Λ. The width of the Gaussian Zr-Zr distribution is given in the lower part. The parameters were obtained by fits in real space to standards of sputtered films of Zr and $Nb_{0.9}Zr_{0.1}$ using a fitting range of 2.35–3.15 Å. The indicated error bars were obtained as described in the text—the true errors could be larger. The errors in the total coordination number are not drawn—they would be a combination of those of the individual coordination numbers.

D. Fit results

To obtain quantitative results, the $\phi(r)$'s for the multilayers were fitted to those of standards. For large Λ's, it was sufficient to use one-Gaussian fits, i.e., to compare the EXAFS for Nb and Zr in multilayers with those of the pure films of Nb and Zr. These one-Gaussian fits for the EXAFS at the Nb edge degraded gradually as Λ decreased. For the Zr-edge data, on the other hand, acceptably small quality-of-fit parameters, R values, were obtained when Λ was large. However, for Λ less than about 100 Å, the fits to a one-Gaussian (Zr-Zr) peak became worse with rapidly growing R values. They became completely unacceptable for Λ less than about 50 Å. Evidently, the Nb and Zr layers behave differently as the multilayer period decreases. We have already argued that the Zr layers (more or less) transform to a bcc structure as their thicknesses become small.

Better fits with much smaller R values were obtained with two-Gaussian fits. In these, we used the $\phi(r)$'s of the Nb (or Zr) film and of the $Nb_{0.2}Zr_{0.8}$ (or $Nb_{0.9}Zr_{0.1}$) alloy film for the Nb-Nb (Zr-Zr) and Nb-Zr (Zr-Nb) signatures. Physically unreasonable sets of parameter values could be obtained with reasonable R values and were excluded. The uncertainties in the parameters presented in the diagrams are determined as the ranges within which the R value changes by a factor of 2 from the minimum value, with the other parameters held fixed.

The results of the fits are summarized in Figs. 4 and 5 for the environments of Zr and Nb absorbers, respectively. For the Zr-edge data we used a six-parameter fit (two sets of numbers of nearest neighbors, distances, and spreads in distances) since the hcp and bcc phases have different numbers of nearest neighbors. In the case of Nb, we could restrict the number of fit parameters to five since the number of nearest neighbors is the same if the Nb absorber sits in a bcc Zr or Nb environment. (We neglect the relatively few numbers of Nb atoms in an hcp Zr environment.)

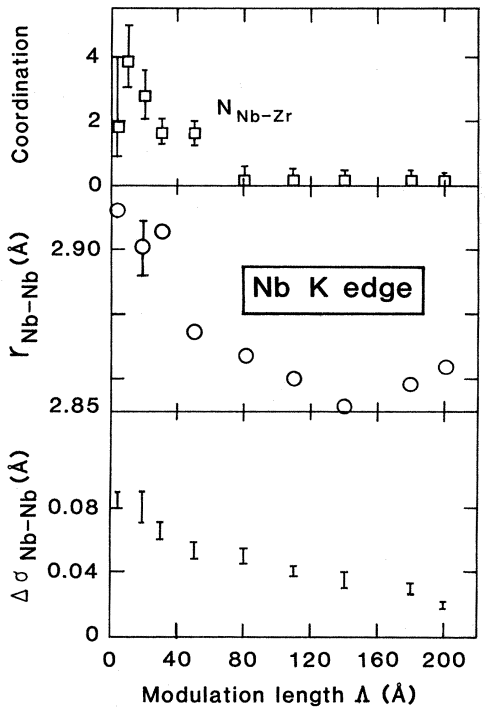

FIG. 5. Average number of Zr neighbors to a Nb absorber, the Nb-Nb distance, and the width in the Nb-Nb distribution as a function of multilayer period. The EXAFS fits were performed in r space over a range 2.2–2.85 Å, utilizing sputtered films of Nb and $Nb_{0.2}Zr_{0.8}$ as standards. It was assumed in the fit that the sum of Zr and Nb neighbors to the Nb absorber equals 8.

For the Zr-edge fits there was a complication. We used the hcp Zr signature from the Zr film to fit the Zr-Zr scattering in the multilayers. This is the correct signature for the large-Λ films where the overwhelming majority of the Zr absorbers are in an hcp environment. However, for the smallest Λ's, the Zr atoms (or most of them) reside in a bcc environment. Then it is not appropriate to use a signature that does not take into account the next-nearest-neighbor shell—the first two shells are quite close together for the bcc structure. We have modified our fitting procedure for the Zr-edge and small-Λ data in two ways. The first way was to shrink the range of the fit in r space such that the contribution from the second shell was deaccentuated. The smaller range meant that the results became less reliable. The second way was to use the $\phi_{Zr}(r)$ of the bcc-structured $Nb_{0.2}Zr_{0.8}$ alloy as the signature for Zr in a bcc Zr environment and the one of $Nb_{0.9}Zr_{0.1}$ for Zr in a bcc Nb environment. This procedure gave good results for $\Lambda < 50$ Å, but poor results for $\Lambda \geq 50$ Å where Zr resides mainly in an hcp environment. Good fits were obtained for the 4- and 19-Å-period layers and the parameters agreed with those from the first procedure. Both of these procedures yielded parameters in good agreement with those from fits using the hcp Zr-Zr standard, particularly the near-neighbor distances. (The fits are more sensitive to changes in the neighbor distances than to changes in amplitudes.) A discrepancy, however, was noted for the $\Lambda = 31$ Å sample. The fit with the bcc Zr standard gave fewer Nb neighbors to the central Zr atom than the hcp Zr standard did. However, for $\Lambda = 31$ Å we are in the middle of the transformation region for hcp to bcc Zr, and in view of the agreement for the other Λ's, we think the results obtained with the hcp signature to be the more trustworthy ones for $\Lambda = 31$ Å.

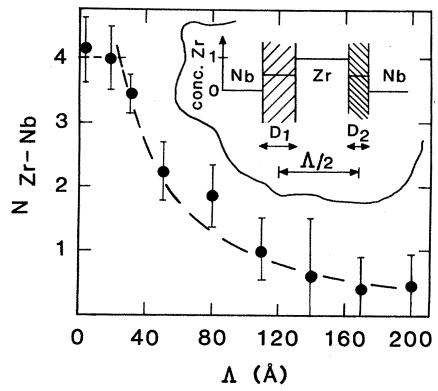

FIG. 6. Extracted number of Nb neighbors to an absorbing Zr atom is compared with a model of interdiffusive regions separating the Nb and Zr layers. The dashed line is the predicted result for interlayers having a 50:50 composition with $D_1 + D_2 = 25$ Å or for a linear diffusion profile with $D_1 + D_2 = 37$ Å.

From Fig. 4 we note that the number of Nb neighbors to a Zr absorber increases continuously from zero as the modulation period decreases. It becomes roughly equal to 4, the average number of Zr neighbors, at the smallest Λ values. The coordination of the majority of the Zr atoms, i.e., the sum of the Nb and Zr neighbors, remains at 12 for large Λ but decreases towards eight as Λ becomes small. Even for the $\Lambda = 19$ Å sample, however, Fig. 4 indicates that part of the multilayer has an hcp environment. The Zr-Zr distance stays essentially at the hcp value until $\Lambda \approx 50$ Å, when its average value diminishes rapidly towards the bcc value. The same value is approached by the Zr-Nb distance. The spread in the Zr-Zr separation, $\sigma_{Zr\text{-}Zr}$, increases at the same time. These results are consistent with the x-ray-diffraction data.[6] They both give definitive evidence for the hcp-to-bcc transition of the Zr layers as Λ becomes less than 50 Å.

The average number of Zr atoms surrounding a Nb absorber remains very low as Λ is decreased to a value of about 80 Å. It then increases, as depicted in Fig. 5, towards a value 4, characteristic of a bcc random alloy ($\Lambda \to 0$). The average number of unlike neighbors seems to be lower for a Nb atom than for a Zr atom at the same Λ. However, this apparent discrepancy is not significantly outside the uncertainties in the amplitudes. It should be noted that there is an increase in $\sigma_{Zr\text{-}Zr}$ as Λ increases beyond 139 Å. Such a change was also observed in the x-ray-diffraction,[6] so it is evidently not an artifact.

IV. INTERLAYER MODEL

In addition to the hcp-to-bcc transition of the Zr layers, the results above indicate that interdiffusive regions separate the Nb and Zr layers. As Λ decreases, the inter-

layer regions become more dominant in the EXAFS spectrum and the average number of unlike neighbors to the absorbing atom increases continuously. Hence it is not sufficient to only consider Zr-Zr (and Nb-Nb) backscattering.

A general expression for the number of unlike neighbors to the central atom can be written down for an arbitrary interdiffusion profile. The number of unlike-neighbor pairs A-B is proportional to $C_A C_B n$ where C_i is the concentration of atoms of type i, and n is the total number of neighbors to the central atom A. Each of these factors is a function of distance into the film, z, due to the layering and interdiffusion. The EXAFS measures the mean number of B neighbors to an A atom which is then given by

$$\bar{n}_{A\text{-}B}=\frac{\int_0^{\Lambda} C_A(z)[1-C_A(z)]n(z)dz}{\int_0^{\Lambda} C_A(z)dz} . \tag{3}$$

Here $n(z)$ is eight for a bcc phase and 12 for an hcp phase. The integration is over a full period Λ of the multilayer modulation. Also one has that

$$\bar{n}_{A\text{-}A}=\frac{\int_0^{\Lambda} C_A^2(z)n(z)dz}{\int_0^{\Lambda} C_A(z)dz} , \tag{4}$$

so that

$$\bar{n}_{A\text{-}A}+\bar{n}_{A\text{-}B}=\frac{\int_0^{\Lambda} C_A(z)n(z)dz}{\int_0^{\Lambda} C_A(z)dz} . \tag{5}$$

For a multilayer sample that is all one phase, Eq. (5) gives $\bar{n}_{A\text{-}A}+\bar{n}_{A\text{-}B}=n$, as it should.

Let us first consider the case where the average concentration of A atoms equals that for the B atoms, i.e., $\bar{C}_A=\bar{C}_B=\frac{1}{2}$. In this case it is obvious from Eq. (3) that the number of B atoms around A is the same as the number of A atoms around $B(\bar{n}_{A\text{-}B}=\bar{n}_{B\text{-}A})$. Let us further consider the limiting situation where the entire sample is in the bcc phase. In this case $n(z)=8$ for all z and $\bar{n}_{A\text{-}A}+\bar{n}_{A\text{-}B}=8$. We further assume that the interdiffusion profile is linear and that A (taken to be Zr) varies linearly from 0 to 1 over a distance D_1 and from 1 to 0 over a distance D_2. The inequality of D_1 and D_2 allows for asymmetric diffusion profiles. The NbZr and ZrNb interlayers do not necessarily need to be the same. Interdiffusion occurs preferentially during the sputtering process and it is not unreasonable to assume that the diffusion of Zr into an already deposited bcc Nb layer is different from Nb into hcp Zr. For this linear profile, Eq. (3) yields

$$\bar{n}_{\text{Zr-Nb}}=\bar{n}_{\text{Nb-Zr}}=\frac{8}{3}\frac{D_1+D_2}{\Lambda} \tag{6}$$

for $D_1+D_2\leq\Lambda$. It is obvious that if $D_1+D_2\gg\Lambda$, the linear profile disappears and one has a homogeneous alloy with $\bar{n}_{\text{Zr-Nb}}=\bar{n}_{\text{Nb-Zr}}=4$.

Let us now relax the constraint that $\bar{C}_A=\bar{C}_B=\frac{1}{2}$. For simplicity we consider a simplified model where we have equally thick layers of Nb and Zr separated by interlayers of thicknesses D_1 and D_2 with average Zr concentrations of x_1 and x_2, respectively. We further assume that the interlayers have a bcc structure. Then the average number of unlike nearest neighbors to a Zr atom become approximately

$$\begin{aligned} N_{\text{Zr-Nb}}&=8(1-x_1)P^{\text{Zr}}(D_1)+8(1-x_2)P^{\text{Zr}}(D_2)\\ &=16[x_1(1-x_1)D_1+x_2(1-x_2)D_2]/[\Lambda-D_1(1-2x_1)-D_2(1-2x_2)] , \end{aligned} \tag{7}$$

and correspondingly for a Nb atom,

$$N_{\text{Nb-Zr}}=16[x_1(1-x_1)D_1+x_2(1-x_2)D_2]/[\Lambda+D_1(1-2x_1)+D_2(1-2x_2)] . \tag{8}$$

In Eq. (7), $P^{\text{Zr}}(D_1)$ is the probability of finding a Zr atom in the interlayer D_1. The unequal denominators in Eqs. (7) and (8) allow for unequal $n_{\text{Zr-Nb}}$ and $n_{\text{Nb-Zr}}$. If we require that $\bar{C}_A=\frac{1}{2}$, then the denominators become equal to Λ [i.e., $D_1(1-2x_1)+D_2(1-2x_2)=0$] and $\bar{n}_{\text{Zr-Nb}}=\bar{n}_{\text{Nb-Zr}}$.

If we further simplify the model and assume $x_1=x_2=\frac{1}{2}$, we find that, for $D_1+D_2\leq\Lambda$,

$$N_{\text{Zr-Nb}}=N_{\text{Nb-Zr}}=4(D_1+D_2)/\Lambda ,$$

and for

$$\begin{aligned} &D_1+D_2\geq\Lambda ,\\ &N_{\text{Zr-Nb}}=N_{\text{Nb-Zr}}=4 . \end{aligned} \tag{9}$$

This result differs from the linear-diffusion—profile case in that these are a larger number of unlike neighbors, larger by a factor of $\frac{3}{2}$.

Such relations (linear profile and step profile with $x_1=x_2=\frac{1}{2}$) are sketched in Fig. 6 where the dashed line is drawn for $D_1+D_2=25$ Å for the step profile and $D_1+D_2=37$ Å for the linear profile. The values of $N_{\text{Zr-Nb}}$ extracted from the experiments are also given. For a symmetric profile, a value of $D_1+D_2=25$–37 Å would mean that the diffusion lengths of Nb into Zr and Zr into Nb would be half this value, i.e., of the order of about 15 Å. Such an interdiffusion is consistent with the x-ray-diffraction results.[6] For example, in Fig. 3 of Ref. 6 it is readily seen that $D_1\simeq D_2\simeq 15$ Å for the $\Lambda=51$ Å sample, although the profile shape is more sinusoidal than our trapezoid or step profile. A $N_{\text{Nb-Zr}}\neq N_{\text{Zr-Nb}}$ can be obtained if we assume that $D_1\neq D_2$ and $x_1\neq x_2$. A comparison between Figs. 4 and 5 indicates that the Nb and Zr atoms "see" different numbers of average neighbors of opposite kind. However, the uncertainties in the extracted numbers are large, so that the differences in the number of unlike neighbors cannot be considered to be significant.

V. CONCLUSIONS

We conclude that the Zr layers (in the multilayer) transform to a mainly bcc-symmetry structure at small modulation lengths. This can be caused by the proximity to the bcc Nb neighboring layers pulling the Zr, which by itself is close to the bcc structure. In addition, the interdiffusion of Nb into Zr and Zr into Nb during sample preparation is significant. From a comparison with a simple model, we concluded that the diffusion lengths characterizing the NbZr and ZrNb interlayers is of the order of 15 Å in the sputtered multilayers. Hence, at small Λ the alloying of Zr and Nb becomes substantial, helping to drive Zr bcc, the preferred structure over a large compositional range in the Nb-Zr alloy system. Even if the extent of the interdiffusion becomes of the same order as the modulation period in the multilayer, there is still modulation of the composition, at least down to $\Lambda = 19$ Å.[6]

ACKNOWLEDGMENTS

Part of this work was done at the SSRL which is supported by the National Science Foundation through the Division of Materials Research, and the National Institute of Health through the Biotechnology Resources Program in the Division of Research Resources (in cooperation with the Department of Energy). The project was partly supported by the U. S. Air Force Office of Scientific Research under Contract No. F49620-82-C-0014, the Swedish Natural Science Research Council, and the Swedish Board for Technical Development. The great hospitality shown to one of us (T.C.) by the Xerox Palo Alto Research Center and Stanford University during a visit was greatly appreciated. The SIMS analysis was performed by H. Odelius and the microprobe work by C. Zercher. The Nb-Zr alloys were provided by Shozo Yoshizumi.

[1]W. M. C. Yang, T. Tsakalakos, and J. E. Hilliard, J. Appl. Phys. 48, 876 (1977); S. L. Lehoczky, J. Appl. Phys. 49, 5479 (1978).

[2]B. J. Thaler, J. B. Ketterson, and J. E. Hilliard, Phys. Rev. Lett. 41, 336 (1978); E. M. Gyorgy, J. F. Dillon, Jr., D. M. McWhan, L. W. Rupp, Jr., L. R. Testardi, and P. J. Flanders, 45, 57 (1980); R. M. White and C. Herring, Phys. Rev. B 22, 1465 (1980); T. Jarlborg and A. J. Freeman, Phys. Rev. Lett. 45, 653 (1980).

[3]P. R. Antoniewicz and G. E. Fredericks, Solid State Commun. 12, 23 (1973); I. O. Kulik, 19, 535 (1976); C. G. Granqvist and T. Claeson, 32, 531 (1979); C. R. Spencer, P. Martinoli, E. D. Gibson, J. D. Verhoeven, and D. K. Finnemore, Phys. Rev. B 18, 1216 (1978).

[4]I. K. Schuller, Phys. Rev. Lett. 44, 1597 (1980); W. P. Lowe, T. W. Barbee, Jr., T. H. Gebelle, and D. B. McWhan, Phys. Rev. B 24, 6193 (1981); T. W. Barbee, Jr. (private communication).

[5]For a review, see T. M. Hayes and J. B. Boyce, in *Solid State Physics,* edited by H. Ehrenreich, F. Seitz, and D. Turnbull (Academic, New York, 1982), Vol. 37, pp. 173–351.

[6]W. P. Lowe and T. H. Geballe, this issue, preceding paper, Phys. Rev. B 29, 4961 (1984).

[7]T. W. Barbee, Jr. and D. Keith, in Proceedings of the Workshop on X-ray Instrumentation for Synchrotron Radiation Research, edited by H. Winick and G. Brown, SSRL Report No. 78-04 (unpublished).

[8]P. A. Lee, P. H. Citrin, P. Eisenberger, and B. M. Kincaid, Rev. Mod. Phys. 53, 769 (1981).

[9]T. M. Hayes, J. Non-Cryst. Solids 31, 57 (1978).